Extracting horizons and sequence boundaries from 3D seismic images

Xinming Wu & Dave Hale
Center for Wave Phenomena, Colorado School of Mines, Golden, CO 80401, USA

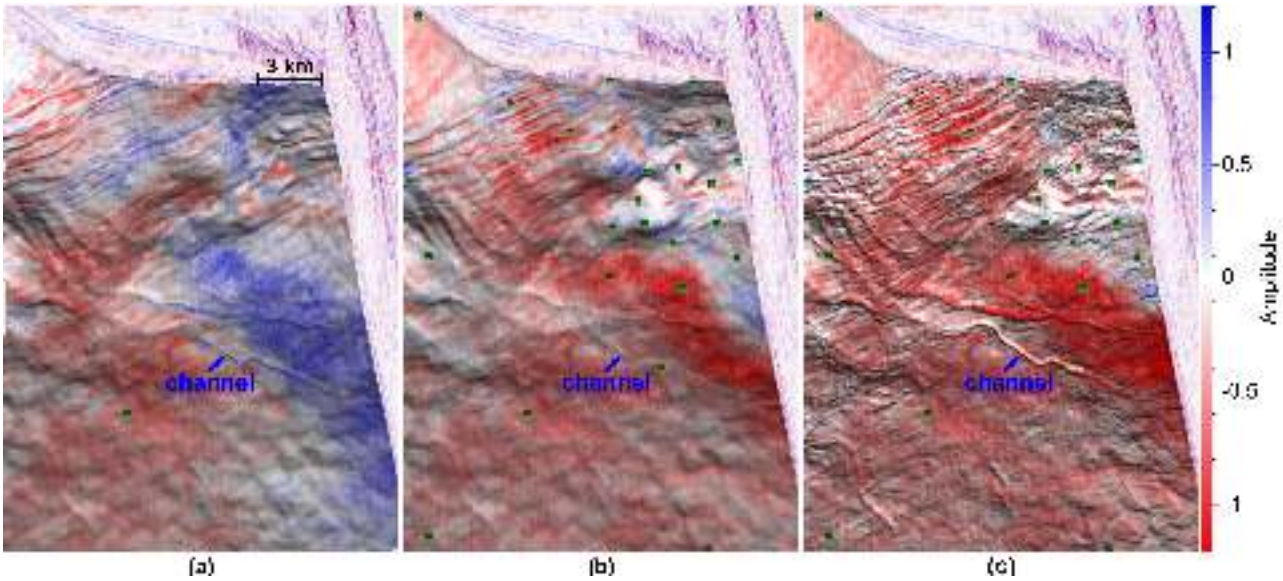

Figure 1. A 3D view of the amplitude-colored seismic horizons (blue, green and red curves in Figure 6) that are extracted using (a) one control point, (b) 25 control points, and (c) 25 control points with refinement using our active-surface method.

ABSTRACT
Horizons and sequence boundaries are important geologically significant surfaces that can be extracted from seismic images. Many automatic methods have been developed to extract horizons, but these methods usually have difficulty extracting horizons that terminate at angular unconformities or sequence boundaries. Using sequence boundaries as constraints is one way to solve this problem, but there exists no automatic method for sequence-boundary extraction. We first introduce a globally optimal method to efficiently extract a horizon from a seismic image. We then use scattered control points as constraints to enable our horizon-extraction method to extract sequence boundaries. Finally, we propose an active-surface method to refine the globally optimized horizons to align with amplitude peaks or troughs and thereby reveal more geologic details.

Key words: horizon sequence boundary control point active surface

1 INTRODUCTION

In 3D seismic images, primary seismic reflectors coincide with geologic interfaces such as stratal surfaces and unconformities with sufficient velocity-density contrasts. A stratal surface is a primary bedding or ancient depositional surface representing a geologically synchronous surface, while an unconformity is a non-depositional or erosional surface separating older strata below from

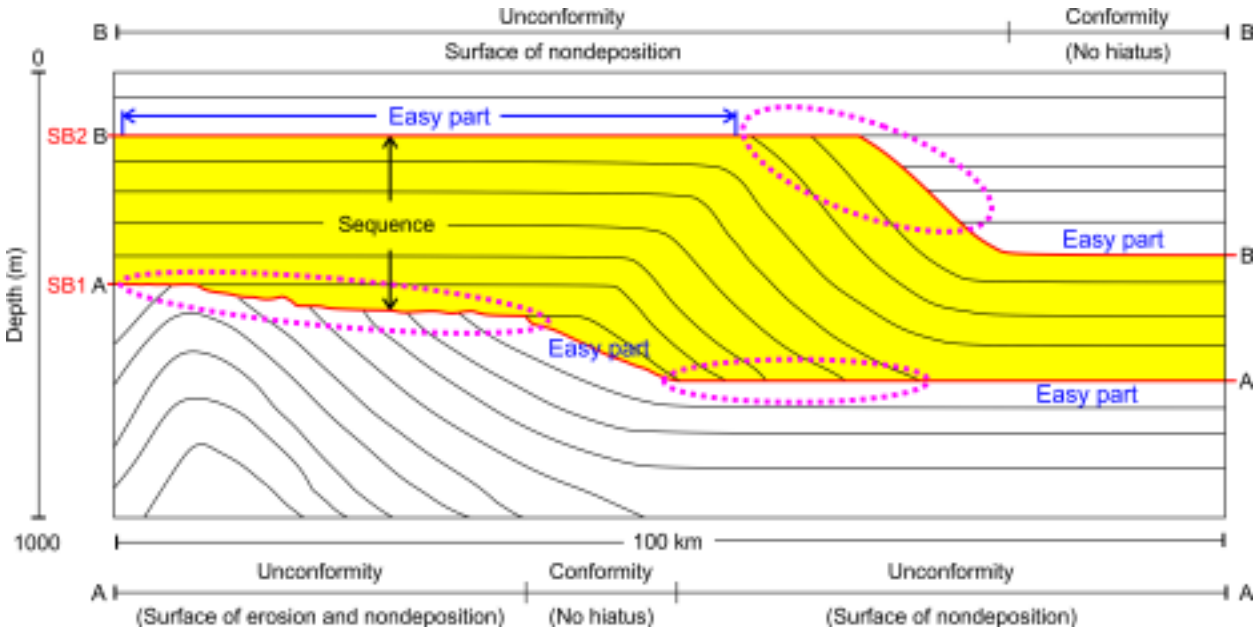

Figure 2. A synthetic sequence stratigraphic model (modified from Mitchum et al. (1977)) containing horizons (black curves) and sequence boundaries (heavy red curves). Ellipses highlight angular unconformities while the easy parts denote conformities and paraconformities.

younger strata above and thus represents a significant gap in geologic time (Vail et al., 1977). Therefore, by tracking or extracting surfaces throughout a 3D seismic image along amplitude peaks or troughs of seismic reflectors, we are able to identify geologically significant surfaces such as horizons and sequence boundaries.

Geologically, horizons (e.g., the black curves in Figure 2) refer to those reflectors representing stratal surfaces. Color-coding of horizons based on amplitude (Figure 1) or other attributes can help reveal ancient depositional environments and geomorphic features (Posamentier et al., 2007). Sequence boundaries (red curves in Figure 2) coinciding with angular unconformities (highlighted by dashed magenta ellipses in Figure 2) can also be extracted along the seismic reflectors, but these represent geologically time-variable surfaces. Sequence boundaries are important in seismic stratigraphic interpretation to define depositional sequences (Mitchum et al., 1977).

One can manually pick horizons and sequence boundaries from 3D seismic images, but this is usually a time-consuming task. To make the process more efficient, methods have been developed to extract horizons automatically. These automated methods, however, cannot extract sequence boundaries, and most fail where horizons terminate at an angular unconformity or sequence boundary.

1.1 Horizon extraction

Automated horizon-extraction methods can be generally classified into three categories. The first is amplitude-based, and extracts horizons by searching the peaks or troughs of seismic reflectors. Coherence or correlation between neighboring traces is usually used to constrain this searching process. Horizons extracted using these methods are helpful for revealing geologic details because they are locally optimal and are thus sensitive to local and small-scale geologic structures. These methods, however, are usually sensitive to noise and limited to simple geology (Hoyes and Cheret, 2011). In addition, they have difficulty extracting horizons that terminate at an angular unconformity or sequence boundary because they do not know how to grow a horizon where truncations, downlaps, onlaps, and toplaps occur.

The second category uses dips (Lomask et al., 2006; Parks et al., 2010) or normal vectors (Luo and Hale, 2012) estimated from seismic reflectors to globally flatten or unfold entire 3D seismic images. These methods obtain all horizons in a seismic image simultaneously and they are more robust for noisy data. However, horizons extracted using these methods are usually smooth and therefore lack detailed geologic structures. In addition, the dips or seismic normal vectors are estimated using locally averaged features of seismic reflectors. While this averaging improves their robustness in noisy data, it degrades their ability to resolute geologic details. These methods also fail to extract horizons that terminate at a sequence boundary because plane-wave de-

struction filters (Claerbout, 1992; Fomel, 2002) or structure tensors (van Vliet and Verbeek, 1995; Fehmers and Höcker, 2003) they use are unable to provide accurate dips or normal vectors at locations where multiple orientations exist in seismic images.

The third category is similar to the second in that it flattens an entire 3D seismic image, but without use of dips or normal vectors. Instead, it uses a relative geologic time (RGT) volume generated by unwrapping a corresponding seismic instantaneous phase image (Stark, 2005; Wu and Zhong, 2012). When globally optimized methods are used to compute an RGT result, these methods yield smooth horizons. Therefore, these methods have similar disadvantages to those of the second category. Wu and Zhong (2012) discuss handling of unconformities by manually interpreting sequence boundaries that serve as constraints. However, the problem remains of how to handle unconformities automatically.

1.2 Sequence boundary extraction

All of the horizon-extraction methods discussed above share the common difficulty in extracting horizons that terminate at an angular unconformity or sequence boundary. One way to solve this problem is to first extract all possible sequence boundaries in a seismic image and then use them as constraints while extracting other horizons. Extracting sequence boundaries would have the added benefit of helping to define depositional sequences. Despite definite benefits in extracting sequence boundaries, however, no method has yet been developed to accomplish this automatically. In manual interpretation of a sequence boundary, interpreters usually first look for angular unconformities (highlighted by magenta dashed ellipses in Figure 2) that imply the presence of sequence boundaries (heavy red curves in Figure 2), and then track the angular unconformities and correlative conformable parts (the easy parts in Figure 2) throughout the seismic image. Angular unconformities in seismic images are landmarks for interpreters who manually pick sequence boundaries; however, they are challenges for automatic methods as discussed above.

1.3 This paper

This paper describes methods for automatically extracting sequence boundaries and horizons in seismic images complicated by noise or chaotic reflectors, and for combining both the orientations and amplitudes of reflectors to obtain globally and locally optimized surfaces.

We first introduce a horizon-extraction method that uses estimated seismic normal vectors. This method uses one control point to indicate the horizon (which contains this point) we want to extract and to initialize a horizontal surface passing through this control point. This initial surface, of course, is inconsistent with the horizon we want to extract. But it is deformed to a different surface whose normal vectors match the seismic normal vectors. Similar to the second category of methods, our method efficiently extracts a globally optimized horizon from a seismic image.

We then discuss the use of control points that constrain our horizon-extraction method to extract sequence boundaries from seismic images. For a sequence boundary, denoted by the red heavy curves in Figure 2, our horizon-extraction method works well for the conformable parts (the easy part in Figure 2), because we can accurately estimate seismic normal vectors for these parts using structure tensors. But the estimated normal vectors at the angular unconformities (highlighted by ellipses in Figure 2) of the sequence boundary are usually not accurate enough to correctly locate the surface at the sequence boundary. We therefore insert several control points at angular unconformities and elsewhere, if necessary. Using a small number of control points, our method can reliably extract a sequence boundary, as well as horizon surfaces where a seismic image is contaminated by noise or where reflectors are chaotic.

Finally, we introduce an *active-surface method* that uses seismic amplitudes to further refine our globally optimized horizon (Figure 1b) to obtain a locally optimized horizon (Figure 1c) with more geologic detail. The active-surface method is similar to the snake or active-contour method proposed by Kass et al. (1988). In contrast to the closed contour used in the snake method, our extracted horizon is an active open surface. Our active-surface method directly uses seismic amplitudes to generate an external force that attracts a horizon to the nearest peaks or troughs in amplitude.

2 HORIZON EXTRACTION FROM SEISMIC NORMAL VECTOR FIELDS

The slopes or normal vectors of seismic reflectors can be used to automatically compute shifts that flatten (Lomask et al., 2006; Parks et al., 2010; Luo and Hale, 2012) a seismic image. Then any seismic horizon can be easily extracted from those shifts. Here we describe a similar method for extracting a single seismic horizon using a seismic normal vector field.

Using structure tensors (van Vliet and Verbeek, 1995; Fehmers and Höcker, 2003), we first compute a field of unit normal vectors $\mathbf{n} = [n_x\ n_y\ n_z]^T$ that are locally perpendicular to seismic reflectors (Luo and Hale, 2012). We then assume a surface $z = f(x, y)$ that was initially horizontal at some specified depth (or time). If we define the surface implicitly by

$$U(x, y, z) = z - f(x, y) = 0, \tag{1}$$

then normal vectors for the surface can be computed as

$$\mathbf{n}_s = \frac{\nabla U(x, y, z)}{\|\nabla U(x, y, z)\|} = \alpha \begin{bmatrix} -f_x \\ -f_y \\ 1 \end{bmatrix}, \tag{2}$$

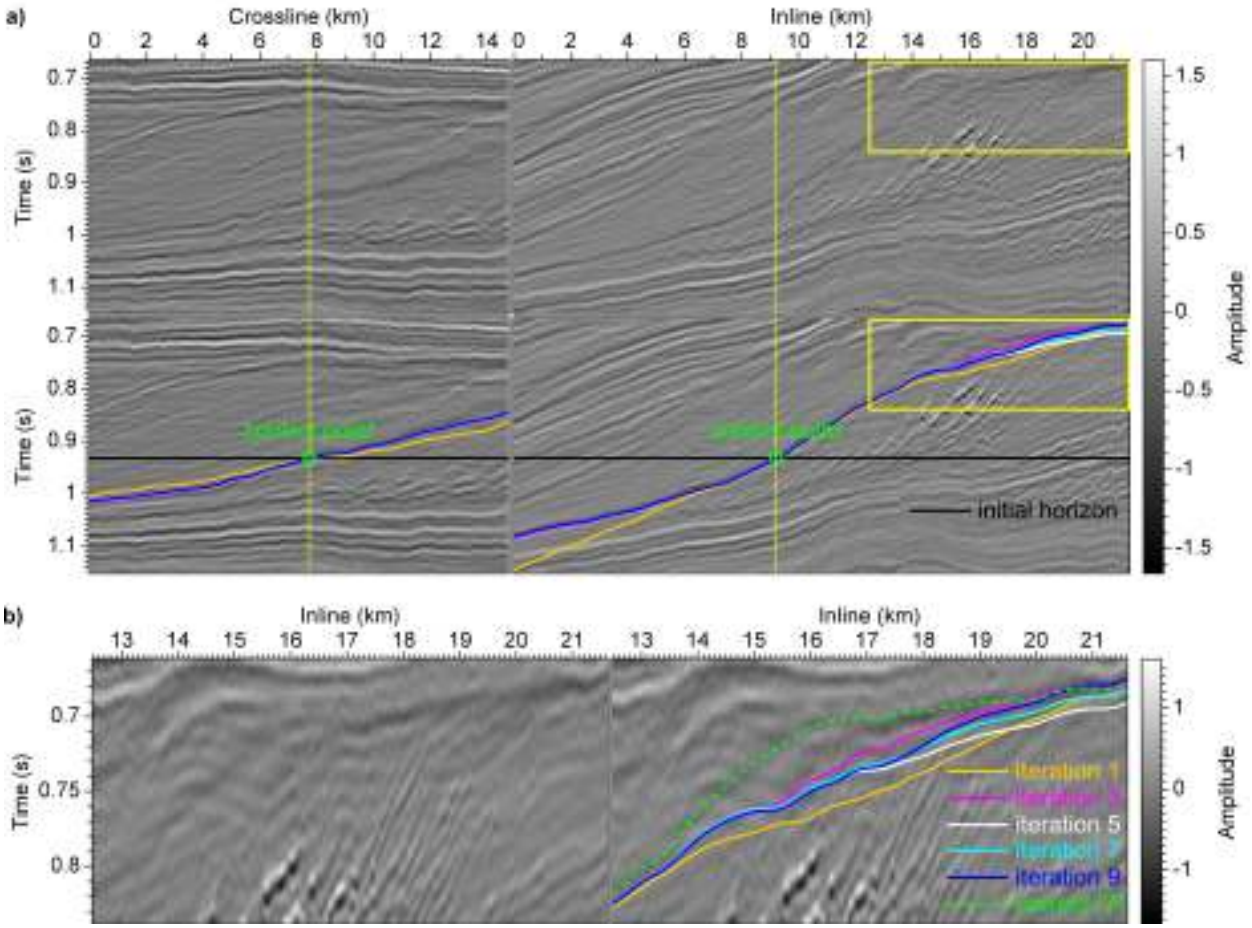

Figure 3. Seismic sections (a) and subsections (b) that intersect with a sequence boundary. The initially horizontal surface (black curve) passes through one control point and is updated iteratively using seismic normal vectors. The dashed green curve denotes the sequence boundary extracted using 26 control points.

where $f_x \equiv \partial f(x,y)/\partial x$, $f_y \equiv \partial f(x,y)/\partial y$, and α is a scale factor to normalize $\mathbf{n}_s$ as unit vectors.

To extract a seismic horizon, we seek to find a surface whose normal vectors $\mathbf{n}_s$ equal the seismic normal vectors $\mathbf{n}$ at corresponding points in the 3D seismic image:

$$\alpha \begin{bmatrix} -f_x \\ -f_y \\ 1 \end{bmatrix} = \begin{bmatrix} n_x \\ n_y \\ n_z \end{bmatrix}. \tag{3}$$

Therefore, setting $\alpha = n_z$, we solve the following inverse-gradient problem to extract the horizon surface $z = f(x,y)$,

$$\begin{bmatrix} f_x \\ f_y \end{bmatrix} = \begin{bmatrix} p \\ q \end{bmatrix}, \tag{4}$$

where $p = -n_x/n_z$ and $q = -n_y/n_z$ are reflector slopes in the x and y directions, respectively. To solve this inverse gradient problem, a common scheme is to minimize the following least-squares cost function (e.g., Horn and Brooks, 1986; Frankot et al., 1988; Horn, 1990; Farnebäck et al., 2007):

$$E = \int\int_\Omega [|f_x - p|^2 + |f_y - q|^2] dxdy. \tag{5}$$

Inspired by Wei and Klette (2002), we modify this cost function by adding a term related to surface curvature:

$$\begin{aligned} E = &\int\int_\Omega \frac{1}{2}(|f_x - p|^2 + |f_y - q|^2) dxdy \\ &+ \frac{\mu}{2}\int\int_\Omega (|f_{xx}|^2 + 2|f_{xy}|^2 + |f_{yy}|^2) dxdy. \end{aligned} \tag{6}$$

This second term is used to improve the robustness of the method for noisy or chaotic seismic reflectors. The value $\mu \geq 0$ weights this surface-curvature term.

To minimize the above cost function E, we use calculus of variations to obtain the Euler-Lagrange equation:

$$\triangle f - \mu \triangle^2 f = \nabla \cdot \mathbf{g}, \tag{7}$$

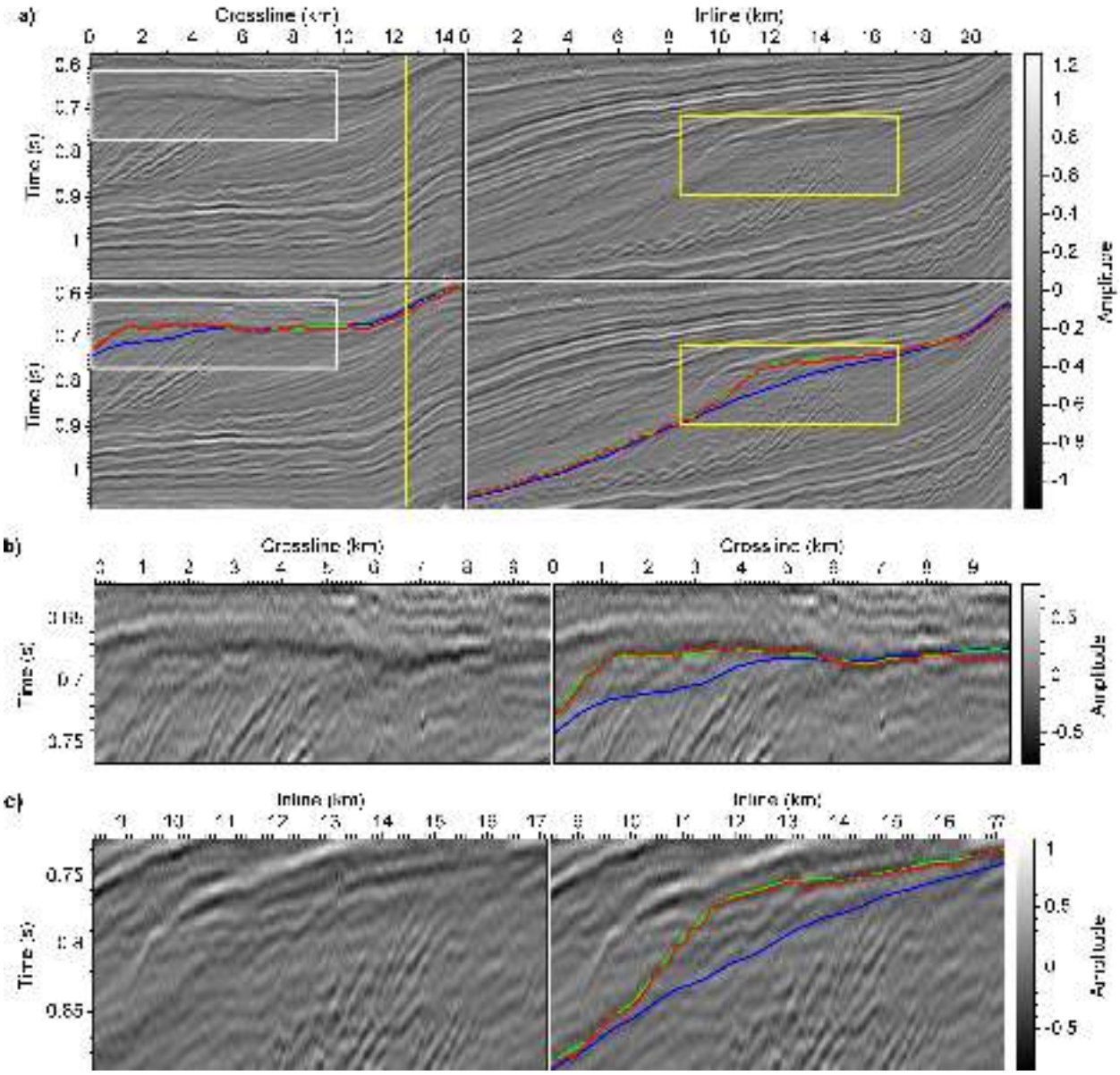

Figure 4. Seismic sections (a) and subsections (b) and (c) corresponding to the white and yellow rectangles, respectively, that intersect with an extracted sequence boundary (the one shown in Figure 3) using one control point (blue curve), 26 control points (green curve), and after refining (red curve) using our active-surface method.

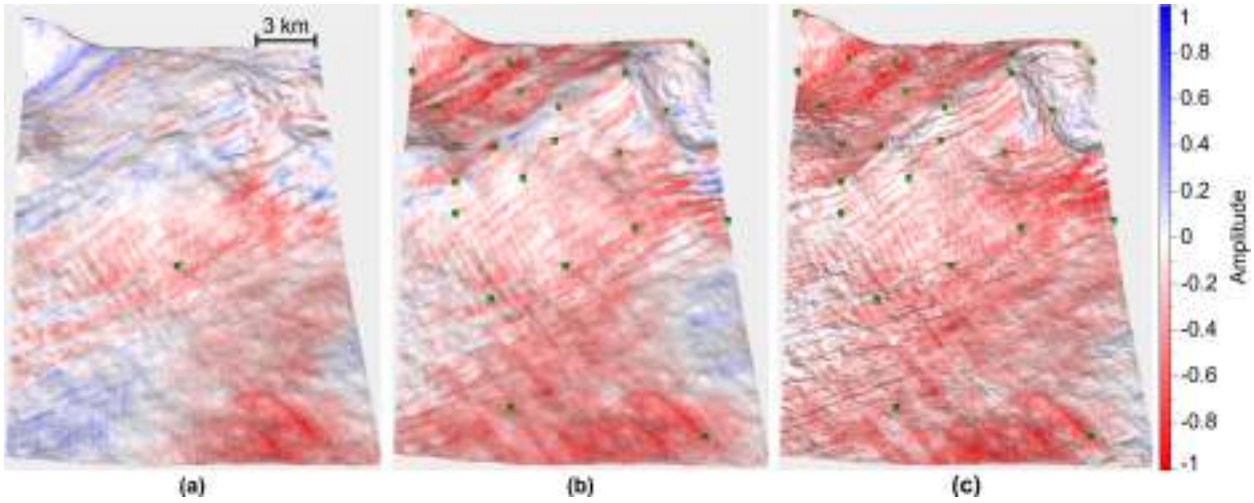

Figure 5. A 3D view of the amplitude-colored sequence boundaries (blue, green and red curves in Figure 4) that are extracted using (a) one control point, (b) 26 control points, and (c) 26 control points with refinement using our active-surface method.

where $\mathbf{g} = [p\ q]^T$ is a vector of reflector slopes, $\triangle f = f_{xx} + f_{yy}$, and $\triangle^2 f = f_{xxxx} + 2f_{xxyy} + f_{yyyy}$. By solving this equation, we can update the surface $z = f(x, y)$ so that its normal vectors $\mathbf{n}_s$ match the seismic normal vectors $\mathbf{n}$ at the current locations of the surface.

Therefore, given an initially horizontal surface (black curves in Figure 3) that is inconsistent with any seismic reflector, our method iteratively reduces the difference between the normal vectors of the surface $\mathbf{n}_s$ and the seismic normal vectors $\mathbf{n}$ at surface locations (x, y, z) to obtain a seismic horizon surface (blue curves in Figure 3).

In Figure 3, using only one control point to indicate which horizon we want to extract, our method deforms the initially horizontal surface to the more nearly correct seismic horizon (blue curves in Figure 3) after 9 iterations. However, in the subsections shown in Figure 3b, we observe that this method fails to deform the surface to the location of the angular unconformity (green dashed curve in Figure 3b). Extracting such a sequence boundary or unconformity is an important but difficult problem for automatic seismic interpretation. Using structure tensors, we fail to estimate the correct normal vector field at an unconformity, but instead compute a smoothed one that yields the incorrect horizon surface shown in Figure 3b. In the next section, we will describe a method to correctly extract a sequence boundary using 26 control points.

3 HORIZON CORRECTION USING CONTROL POINTS

In the previous section we described a seismic horizon-extraction method based on seismic normal vectors. Near unconformities, or in areas the image is noisy, the estimated normal vector field is not reliable enough to extract a correct horizon, sequence boundary, or unconformity. In such cases, instead of using a fully automatic method, we might manually interpret the seismic image to obtain a more geologically reasonable surface. However, we need not manually interpret the entire horizon. Using a small number of control points, we interpolate a correction for an updating surface described in section 2 to efficiently extract a accurate sequence boundary or horizon in a noisy image.

Suppose we have a set of n control points $(x_i, y_i, z_i), i = 1, 2, \ldots, n$ that are not all collinear. we can impose constraints in our horizon extraction using the method described by Horovitz and Kiryati (2004). In each iteration of horizon updating as described in section 2, we first compute an updated horizon $z = f(x, y)$ using seismic normal vectors, and then use the thin-plate spline interpolation method to interpolate a correction surface $z_c = c(x, y)$ by using the depth difference $z_i - f(x_i, y_i)$ between the control points and the updated horizon. The horizon is then corrected using the interpolated correction field, before the next iteration.

3.1 Thin-plate spline interpolation

Thin-plate spline interpolation is a classic method for interpolation of scattered data to yield a smooth function $c(x, y)$ that minimizes the integral

$$I(c) = \int\int_{\Omega} (|c_{xx}|^2 + 2|c_{xy}|^2 + |c_{yy}|^2) dxdy, \quad (8)$$

while satisfying the interpolation conditions

$$c(x_i, y_i) = z_i,\ i = 1, 2, \ldots, n. \quad (9)$$

Duchon (1977) shows that the interpolating function $c(x, y)$ has the form

$$c(x, y) = a_0 + a_1 x + a_2 y + \sum_{i=1}^{n} w_i \phi(r_i), \qquad (10)$$

where r_i is the distance between the i-th control point (x_i, y_i) and $(x, y) \in \Omega$; $a_0,\ a_1$ and a_2 are the coefficients of the planar term in $c(x, y)$; and

$$\phi(r) = r^2 log(r),\ 0 < r < \infty. \qquad (11)$$

The coefficients w_i satisfy

$$\sum_{i=1}^{n} w_i = 0,\ \sum_{i=1}^{n} w_i x_i = 0,\ \sum_{i=1}^{n} w_i y_i = 0. \qquad (12)$$

From the correction values known at the control points,

$$c(x_i, y_i) = z_i - f(x_i, y_i), \qquad (13)$$

we can compute the coefficients in equation 10 by solving the system of linear equations:

$$\begin{bmatrix} \mathbf{K} & \mathbf{P} \\ \mathbf{P}^T & \mathbf{O} \end{bmatrix} [\mathbf{W}|a_0\ a_1\ a_2]^T = [\mathbf{C}|0\ 0\ 0]^T, \qquad (14)$$

where

$$\mathbf{K} = [\phi(r_{ij})]_{n\times n},\ r_{ij} = |(x_i, y_i) - (x_j, y_j)|, \qquad (15)$$

$$\mathbf{P} = \begin{bmatrix} 1 & x_1 & y_1 \\ 1 & x_2 & y_2 \\ \vdots & \vdots & \vdots \\ 1 & x_n & y_n \end{bmatrix}_{n\times 3}, \quad \mathbf{O} = \begin{bmatrix} 0 & 0 & 0 \\ 0 & 0 & 0 \\ 0 & 0 & 0 \end{bmatrix}_{3\times 3}, \qquad (16)$$

$$\mathbf{W} = [w_1\ w_2\ \ldots\ w_n]_{1\times n}, \qquad (17)$$

and

$$\mathbf{C} = [c(x_1, y_1)\ \ c(x_2, y_2)\ \ \ldots\ \ c(x_n, y_n)]_{1\times n}. \qquad (18)$$

With the coefficients $[\mathbf{W}\ a_0\ a_1\ a_2]$, we can use equation 10 to interpolate correction values $c(x, y)$ at every (x, y) for which the surface is defined. The updated horizon $f(x, y)$ using seismic normal vectors is then

$$f_c(x, y) = f(x, y) + c(x, y). \qquad (19)$$

This corrected horizon $f_c(x, y)$, which now honors the control points, is then used for the next iteration.

3.2 Results using control points

When the normal vectors estimated using structure tensors are inaccurate (e.g., near unconformities, noisy data, and chaotic reflectors), the use of control points helps to extract a more reliable horizon or sequence boundary.

As shown in Figure 3, when we extract the sequence boundary passing through the control point (green circle in Figure 3a), the surface we extract (blue curves in Figure 3) matches well with reflectors in the conformable areas (left-side section and the left part of the right-side section in Figure 3a) where normal vectors can be estimated accurately. However, the extracted surface (blue curves) at the unconformity area (Figure 3b) is deflected from the corrected position (dashed green curve in Figure 3b) because estimated normal vectors at that area are inaccurate. Using 26 control points (green points in Figure 5b), we compute a more accurate sequence boundary (dashed green curve in Figure 3b). Figure 4 shows two different seismic sections that intersect with the sequence boundary extracted by using one control point (blue curves), 26 control points (green curves), and further refined (red curves) using the active-surface method discussed below. We observe that the sequence boundary extracted using 26 control points correctly follows the unconformity while the one using only one control point does not. Figure 5 shows the extracted sequence-boundary surface colored with amplitudes. Amplitude values for 26 control points (Figure 5b) are more uniform than for one control point (Figure 5a).

Moreover, with use of more control points, an initially horizontal surface converges more quickly to a seismic reflector. For example, it takes nine iterations to converge (blue curves in Figure 4) using one control point but only five iterations to converge (green curves in Figure 4) using 26 control points.

4 HORIZON REFINEMENT USING ACTIVE-SURFACE METHOD

Horizons extracted using amplitude-based methods are often locally correct but are sensitive to noise and usually accurate for only simple geology (Hoyes and Cheret, 2011). Our horizon-extraction method and other methods that use orientations (Lomask et al., 2006; Parks et al., 2010; Luo and Hale, 2012) estimated from seismic images are more robust for noisy data and can extract globally optimal horizons. Because of the global optimization and use of orientations estimated from locally averaged structures, these methods, however, might smooth out some subtle geologic structures or details that can be important in geologic interpretations. To reveal more subtle geologic structures or events in a horizon, we developed an active-surface method to refine extracted horizons.

4.1 Active surface

The active-snake or active-contour model, first introduced by Kass et al. (1988), is a powerful method for detecting closed boundary curves in 2D image segmentations. The active snake method is based on energy-minimizing spline curves influenced by internal forces and external image forces. The external image forces

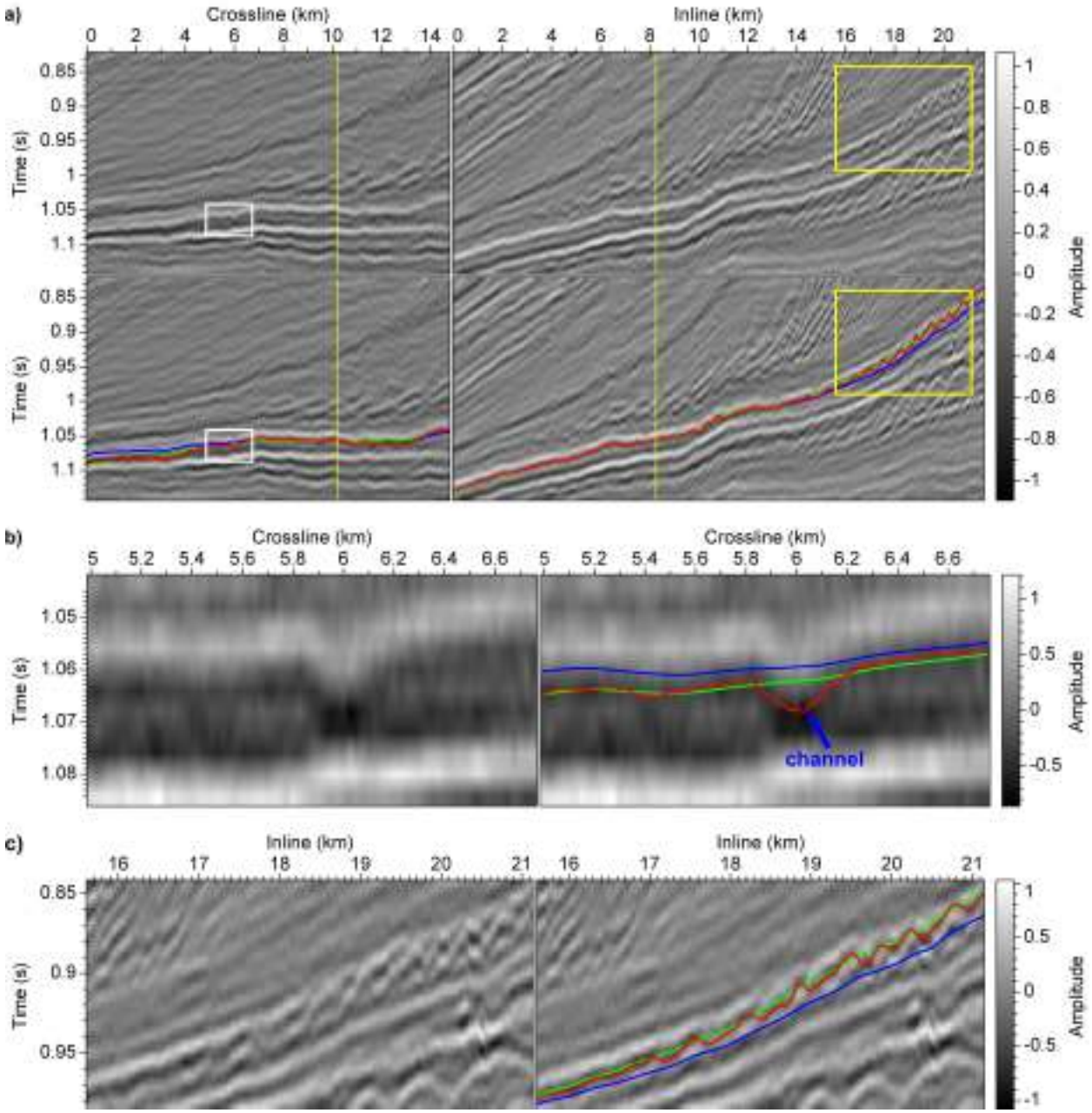

Figure 6. Seismic sections (a) and subsections (b) and (c) corresponding to the white and yellow rectangles, respectively, that intersect with an extracted seismic horizon (the one shown in Figure 1) using one control point (blue curve), 25 control points (green curve), and after refining (red curve) using our active-surface method.

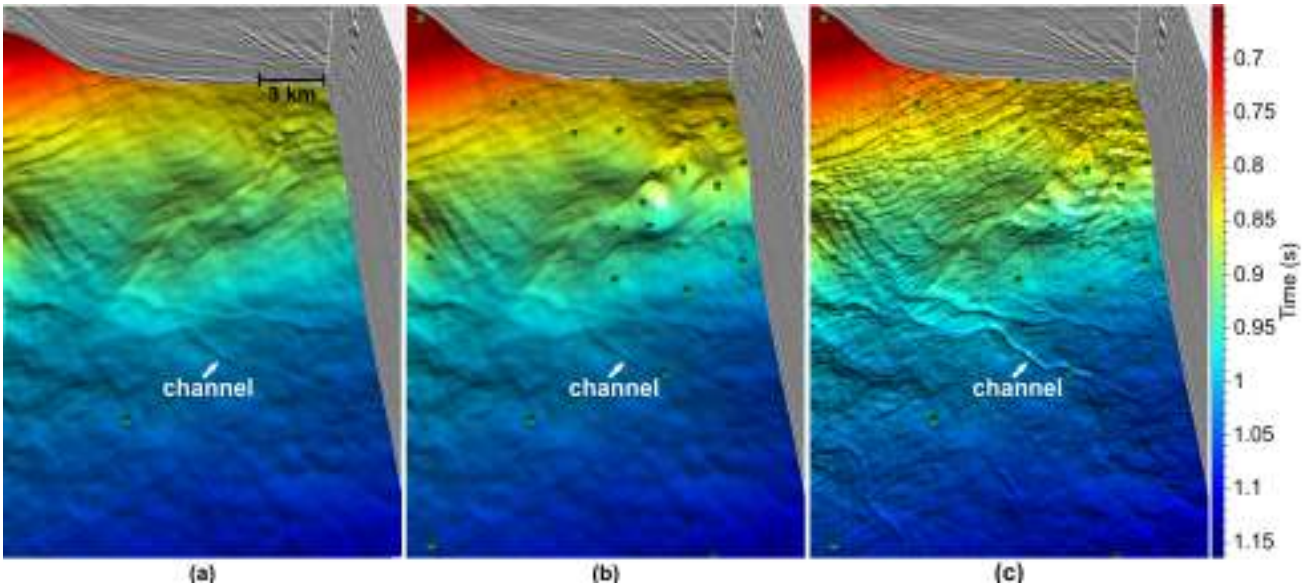

Figure 7. A 3D view of the time-colored horizons (blue, green and red curves in Figure 6) that are extracted using (a) one control point, (b) 25 control points, and (c) 25 control points with refinement using our active-surface method.

pull an initial contour to nearby edges in the 2D image, while the internal forces preserve the original shape and smoothness of the contour. Chopra and Marfurt (2008) suggest that the active-snake or active-contour method might be used to detect channels and other stratigraphic features. In this paper, we discuss an active surface which is an open surface that deforms vertically to align with nearby peaks or troughs in seismic amplitude.

Using seismic normal vectors, control points, and the methods described above, we obtain a globally optimized horizon that is consistent with reflector structure is not necessarily aligned with seismic peaks or troughs. We seek to deform the extracted horizon $z = f(x, y)$ to be aligned with the seismic peaks or troughs. Considering the horizon as an active surface, we define the energy of the active surface using an internal energy term E_{int} and an external energy term E_{ext}:

$$E(f, A) = \beta E_{int}(f) + E_{ext}(A), \tag{20}$$

where A is a 3D seismic image and β builds a trade-off between the internal and external energy terms. By minimizing this energy function, we can align the horizon with nearby seismic peaks or troughs.

The internal energy of the active surface is defined by its bending energy using the surface curvature approximation shown in equation 6 and 8:

$$E_{int}(f) = \int\int_{\Omega} \frac{1}{2}(|f_{xx}|^2 + 2|f_{xy}|^2 + |f_{yy}|^2)dxdy. \tag{21}$$

The external energy of the active surface is defined by its position in a seismic image:

$$E_{ext}(A) = \int\int_{\Omega} \pm A(x, y, f(x, y))dudv. \tag{22}$$

To align the horizon $z = f(x, y)$ with seismic troughs we simply use the seismic amplitude $A(x, y, f(x, y))$; to align with seismic peaks we use $-A(x, y, f(x, y))$.

Assume we want the horizon to be aligned with seismic troughs. Then the total energy of the active surface is

$$E(f, A) = \int\int_{\Omega} [\frac{\beta}{2}(|f_{xx}|^2 + 2|f_{xy}|^2 + |f_{yy}|^2) + A(x, y, f(x, y))]dxdy. \tag{23}$$

We consider only the vertical deformation of the active surface; then we can use calculus of variations to equalize the minimization of the above energy function by solving the Euler-Lagrange equation:

$$\beta\triangle^2 f + \frac{\partial A}{\partial z}|_{z=f(x,y)} = 0. \tag{24}$$

By solving this equation, an extracted horizon can be further refined to align with nearby seismic troughs.

4.2 Results for the active-surface method

In Figure 6, observe that the extracted horizon (green curves) using 25 control points is closer the seismic troughs than the one (blue curves) using only one control point, but both horizons are locally smooth and are not aligned with troughs in Figures 6b and 6c. Because these horizons are extracted using a globally optimal method and normal vectors estimated from averaged reflector structures, we obtain smooth horizon surfaces as shown in Figures 7a and 7b. Even though local amplitude variations indicate small geologic structures in horizons shown in Figures 1a and 1b, the shapes of those

small geologic structures cannot be seen in the horizons (Figures 7a and 7b, Figures 1a and 1b).

After applying our active-surface method to the globally optimized horizons (green curves in Figures 4 and 6), we obtain refined horizons (red curves in Figures 4 and 6) that are well aligned with troughs in seismic amplitude, as expected. In the 3D visualizations of the refined horizons (Figures 1c, 5c and 7c), we see many subtle geologic structures that cannot be seen in the unrefined horizons (Figures 1a and 1b, 5a and 5b, 7a and 7b). For example, channel structures appearing in a seismic image can be difficult to detect using just seismic normal vectors estimated from structure tensors. Therefore, globally optimized horizons extracted using normal vectors, but without using the active-surface method, fail to detect the incised valley of a subtle channel appearing in Figure 6b and marked in Figures 1 and 7. Although we observe some amplitude variations that indicate the existence of a channel in the globally optimized horizons (Figures 1a and 1b), the incised valley structure of the channel is not apparent. After refinement using the active-surface method, we clearly see the cross-section of the incised channel in the horizon (red curve in Figure 6b). The incised valley structure and shape of the channel are readily and continuously apparent in both the time- (Figure 7c) and amplitude-colored (1c) horizons.

5 CONCLUSION

We have developed methods to extract globally optimal horizons using seismic normal vectors, to extract sequence boundaries using control points, and to refine extracted horizons to align with seismic peaks or troughs using an active-surface method. Our horizon-extraction method is flexible for extracting any horizon we choose in a seismic image by using one control point that indicates the chosen horizon. When we sparsely define control points at angular unconformities, the horizon-extraction method can be improved to extract sequence boundaries. Of course, we can also choose control points in complicated areas with noise or chaotic reflectors to extract more reliable horizons in such areas. Using the active-surface method, extracted horizons can be aligned with seismic peaks or troughs to reveal more geologic detail.

Our methods can be further improved. Firstly, instead of using a small-dip approximation for surface curvatures, as in all the methods we describe here, we can use a more accurate one. Secondly, the step of horizon refinement using active-surface methods was separated from the step of horizon extraction using normal vectors; we can combine the two steps together to extract a horizon that honors both seismic amplitudes and orientations. Thirdly, our methods extract single horizons or sequence boundaries from a seismic image one at a time, but processing an entire seismic image is perhaps more useful, and we should modify our method to do this. Finally, we use control points to allow our method to avoid difficulties in horizon extraction at angular unconformities. However, estimating accurate normal vectors at angular unconformities is a preferable solution to this problem and would enable a completely automatic method for sequence-boundary extraction.

ACKNOWLEDGMENTS

We thank the sponsor companies of the Consortium Project on Seismic Inverse Methods for Complex Structures, whose support made this research possible. The 3D seismic images shown in this paper were provided by dGB Earth Sciences. Thanks to Ken Larner and Diane Witters for reviewing and revising this paper. Xinming thanks all C-team members and Luming Liang for their help with Java and Mines Java Toolkit (JTK) during his research.

REFERENCES

Chopra, S., and K. J. Marfurt, 2008, Emerging and future trends in seismic attributes: The Leading Edge, **27**, 298–318.

Claerbout, J. F., 1992, Earth soundings analysis: Processing versus inversion: Blackwell Science.

Duchon, J., 1977, Splines minimizing rotation-invariant semi-norms in sobolev spaces: Constructive Theory of Functions of Several Variables, Springer Berlin Heidelberg, 85–100.

Farnebäck, G., J. Rydell, T. Ebbers, M. Andersson, and H. Knutsson, 2007, Efficient computation of the inverse gradient on irregular domains: 2007 IEEE 11th International Conference on Computuer Vision, Vols 1-6, IEEE, 2710–2717.

Fomel, S., 2002, Applications of plane-wave destruction filter: Geophysics, **67**, 1946–1960.

Frankot, R. T., R. Chellappa, and S. Member, 1988, A method for enforcing integrability in shape from shading algorithms: IEEE Transactions on Pattern Analysis and Machine Intelligence, **10**, 439–451.

Horn, B. K. P., 1990, Height and gradient from shading: International Journal of Computer Vision, **5**, 37–75.

Horn, B. K. P., and M. J. Brooks, 1986, The variational approach to shape from shading: Computer Vision, Graphics, and Image Processing, **33**, 174–208.

Horovitz, I., and N. Kiryati, 2004, Depth from gradient fields and control points: bias correction in photometric stereo: Image and Vision Computing, **22**, 681–694.

Hoyes, J., and T. Cheret, 2011, A review of global interpretation methods for automated 3D horizon picking: The Leading Edge, **30**, 38–47.

Kass, M., A. Witkin, and D. Terzopoulos, 1988,

Snakes: Active contour models: International Journal of Computer Vision, **1**, 321–331.
Lomask, J., A. Guitton, S. Fomel, J. Claerbout, and A. A. Valenciano, 2006, Flattening without picking: Geophysics, **71**, 13–20.
Luo, S., and D. Hale, 2012, Unfaulting and unfolding 3D seismic images: CWP Report 722.
Fehmers, G. C., and C. Höcker, 2003, Fast structural interpretation with structure-oriented filtering: Geophysics, **68**, 1286–1293.
Mitchum, R. M., P. R. V. Jr., and S. Thompson, 1977, Seismic stratigraphy and global changes of sea level: Part 2. the depositional sequence as a basic Unit for stratigraphic analysis: Section 2. application of seismic reflection configuration to stratigraphic interpretation: M 26: Seismic Stratigraphy-Applications to Hydrocarbon Exploration, AAPG Memoirs, 53–62.
Parks, D., C. S. of Mines. Dept. of Mathematical, and C. Sciences, 2010, Seismic image flattening as a linear inverse problem: Colorado School of Mines.
Posamentier, H., R. Davies, J. Cartwright, and L. Wood, 2007, Seismic geomorphology - an overview: in: R.J. Davies, H.W. Posamentier, L.J. Wood, J.A. Cartwright (Eds.), Seismic Geomorphology, Geological Society of London Special Publication, 1–14.
Stark, T. J., 2005, Generating a seismic Wheeler volume: 75th Ann. Internat. Mtg., Soc. of Expl. Geophys., 782–785.
Vail, P. R., R. G. Todd, and J. B. Sangree, 1977, Seismic stratigraphy and global changes of sea level: Part 5. chronostratigraphic significance of seismic reflections: Section 2. application of seismic reflection configuration to stratigraphic interpretation: M 26: Seismic Stratigraphy-Applications to Hydrocarbon Exploration, AAPG Memoirs, 99–116.
van Vliet, L. J., and P. W. Verbeek, 1995, Estimators for orientation and anisotropy in digitized images: ASCI95, Proc. First Annual Conference of the Advanced School for Computing and Imaging (Heijen, NL, May 16-18), ASCI, 442–450.
Wei, T., and R. Klette, 2002, Height from gradient using surface curvature and area constraints: In 3rd Indian Conference on Computer Vision, Graphics and Image Processing, Ahmedabad, 204–210.
Wu, X., and G. Zhong, 2012, Generating a relative geologic time volume by 3D graph-cut phase unwrapping method with horizon and unconformity constraints: Geophysics, **77**, 21–34.